Supporting Information

Massive Intracellular Remodeling of CuS Nanomaterials Produces Nontoxic Bioengineered Structures with Preserved Photothermal Potential

Alberto Curcio[†,‡], Aurore Van de Walle[†,‡], Emilia Benassai[†,§], Aida Serrano[‖,⊥], Nathalie Luciani[†], Nicolas Menguy[α], Bella B Manshian[//], Ara Sargsian[//], Stefaan Soenen[//], Ana Espinosa[+], Ali Abou-Hassan[§]*, Claire Wilhelm[†,‡]*

[†] Laboratoire Matière et Systèmes, Complexes MSC, UMR 7057, CNRS & University of Paris, 75205, Paris Cedex 13, France.

[‡] Laboratoire PhysicoChimie Curie, Institut Curie, PSL Research University - Sorbonne Université – CNRS, 75005 Paris, France.

[§] Sorbonne Université, CNRS UMR234, PHysico-chimie des Electrolytes et Nanosystèmes InterfaciauX, PHENIX, F-75005 Paris, France.

[‖] Spanish CRG beamline at the European Synchrotron (ESRF), B.P. 220, F-38043 Grenoble, France

[⊥] Departamento de Electrocerámica, Instituto de Cerámica y Vidrio, ICV-CSIC, Kelsen 5, 28049 Madrid, Spain

[α] Sorbonne Université, UMR CNRS 7590, MNHN, IRD, Institut de Minéralogie, de Physique des Matériaux et de Cosmochimie, IMPMC, 4 place Jussieu, 75005 Paris, France.

[//] NanoHealth and Optical Imaging Group, KU Leuven, Department of Imaging and Pathology, Herestraat 49, B3000 Leuven, Belgium

[+] Nanobiotecnología (IMDEA-Nanociencia), Unidad Asociada al Centro Nacional de Biotecnología (CSIC), 28049 Madrid, Spain

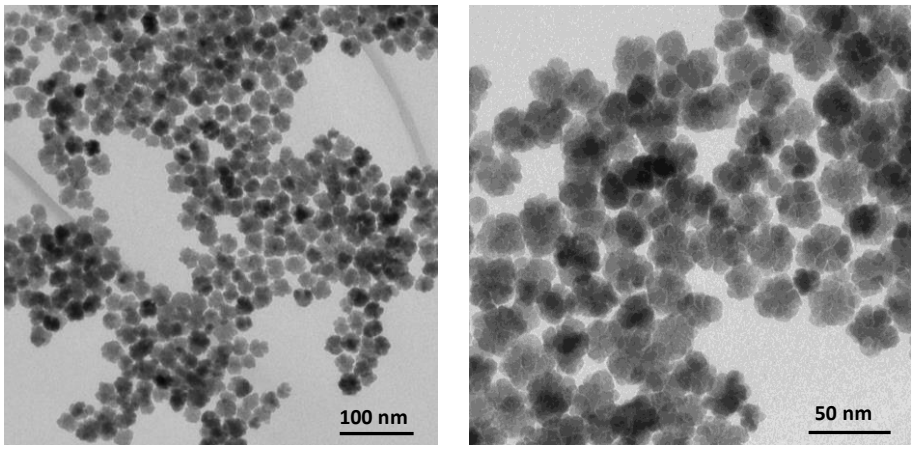

Figure S1: Transmission Electron Microscopy (TEM) of the iron oxide nanoflowers (IONF) composing the core of the IONF@CuS hybrid, before encapsulation.

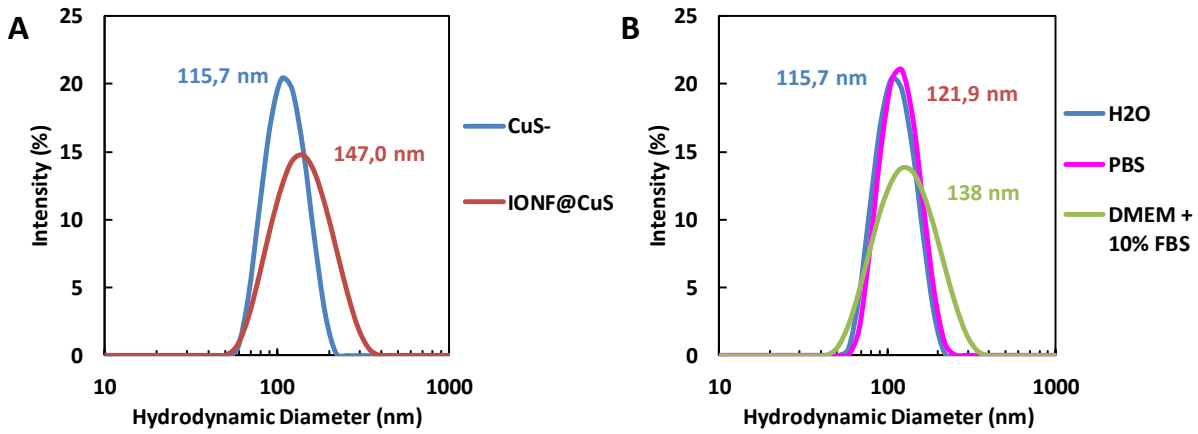

Figure S2: A) Intensity-based DLS analysis of the CuS and IONF@CuS NPs in aqueous dispersion (water) expressed as suspension in water. B) Impact on the hydrodynamic size of the dispersion of the CuS NPs in PBS or in FBS supplemented (10%) culture medium (DMEM).

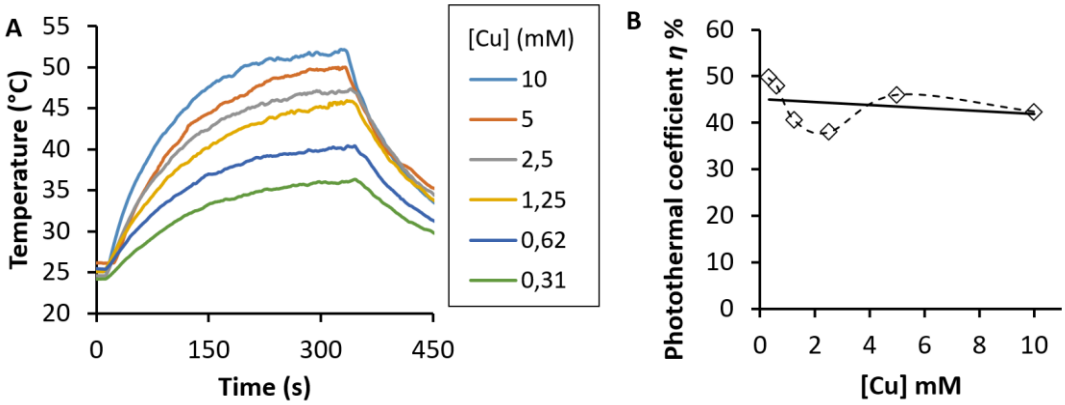

Figure S3: Calculation of the light-to-heat conversion efficiency η of the IONF@CuS according to $\eta = \frac{hA(T_{Max} - T_{Amb}) - Q_{Dis}}{I_0 \cdot S\,(1 - 10^{-A_{1064}})}$ where h is the heat transfer coefficient, A is the area of the container, $T_{Max} - T_{Amb}$ is the temperature change, Q_{Dis} the heat dissipated from light absorbed by the quartz sample cell itself and the solvent, I_0 the incident laser power in W, S the illuminated area in cm^2 and A_{1064} is the NPs absorbance at 1064 nm. These measures were carried out on IONF@CuS NPs aqueous dispersions for 6 different Cu concentrations from 0.2 to 10 mM, and provided a photothermal conversion coefficient of (42 ± 6) %.

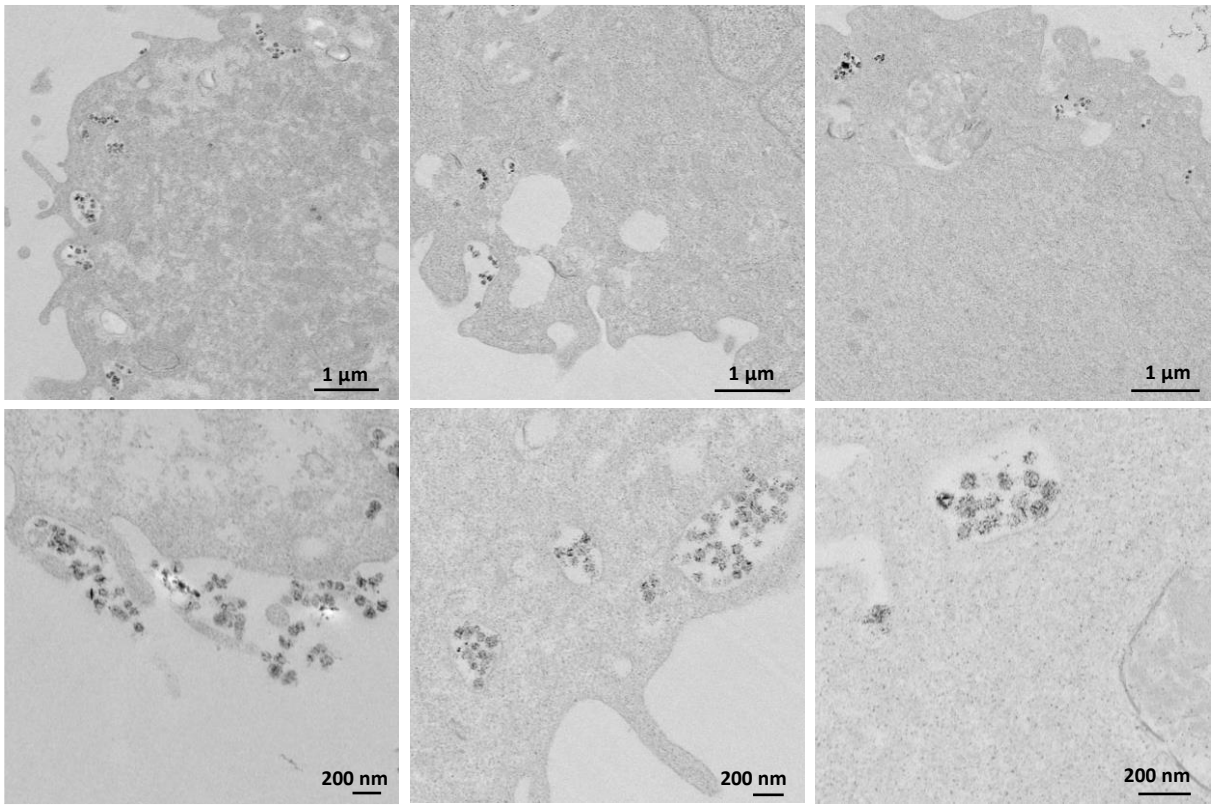

Figure S4: TEM imaging of cells incubated with CuS NPs (day 0). The non-specific interactions between the nanoparticles and the cells are visible at the cell outer membrane, and most NPs are internalized in endosomes.

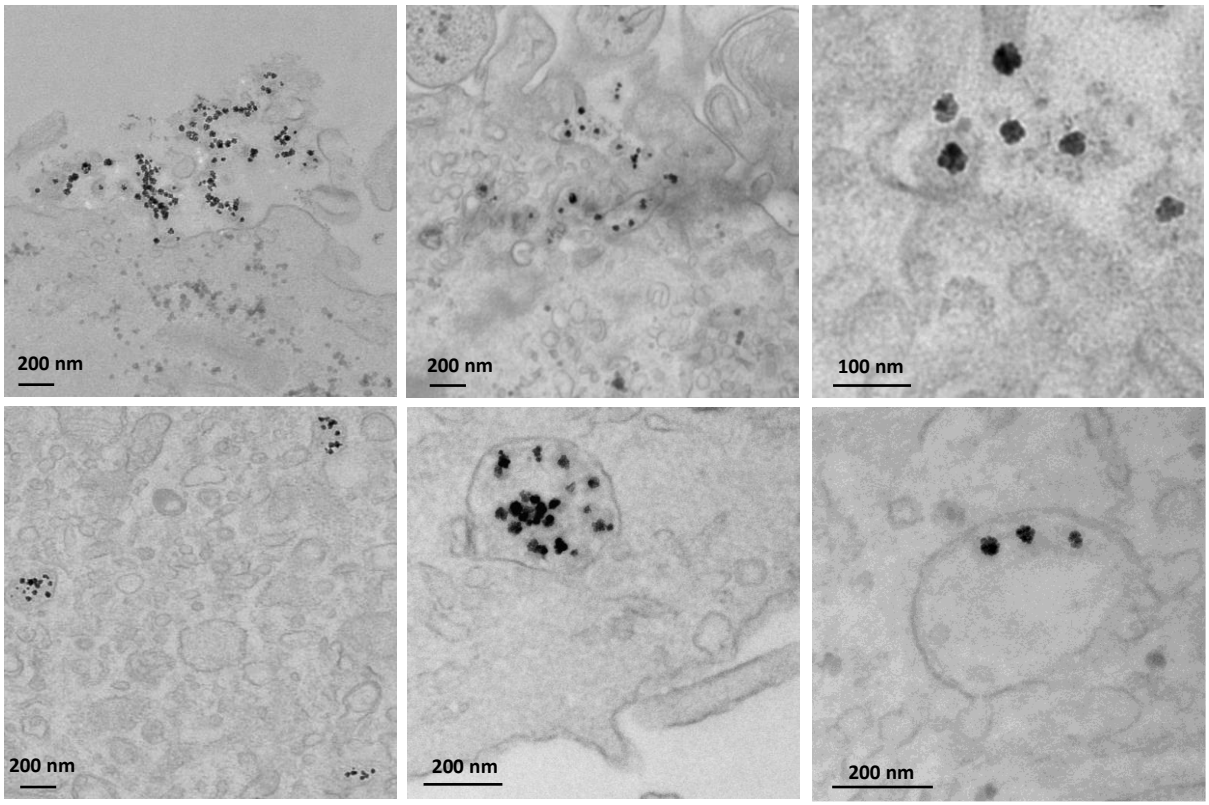

Figure S5: TEM of IONF@CuS at day 0. A similar behavior is observed, with intact NPs at the outer membrane or internalized in endosomes. The different image contrast is due to the presence of IONFs.

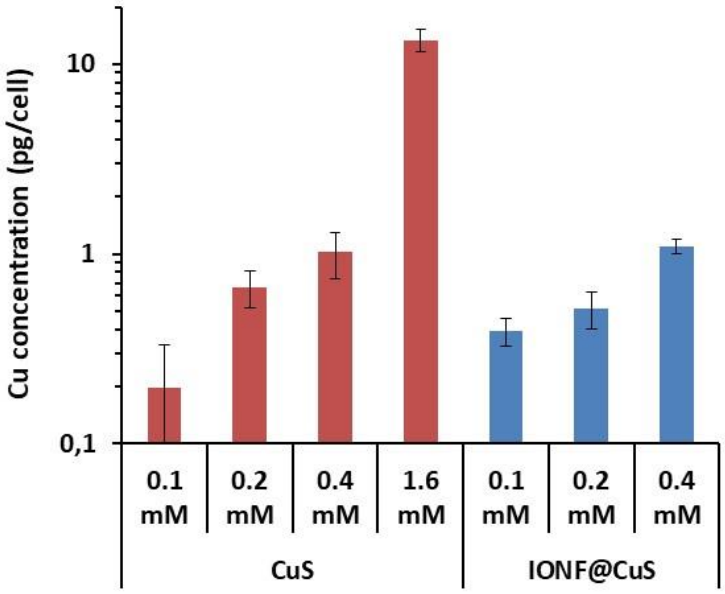

Figure S6: Copper internalization in primary stem cells at day 0, as a function of the extracellular concentration upon 4 hours internalization, quantified by elemental analysis (ICP-AES).

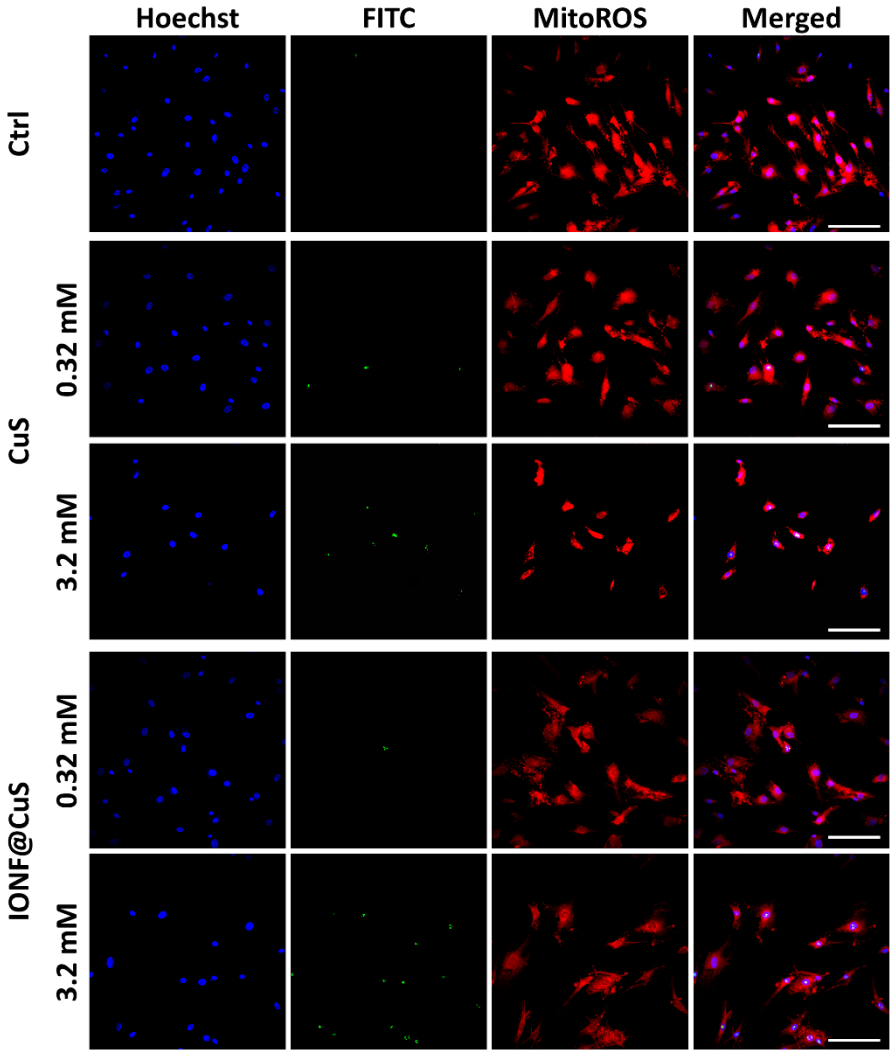

Figure S7: Representative images of viability and mitochondrial ROS staining used for the Incell analyser microscopy system. Scale bar = 200 µm.

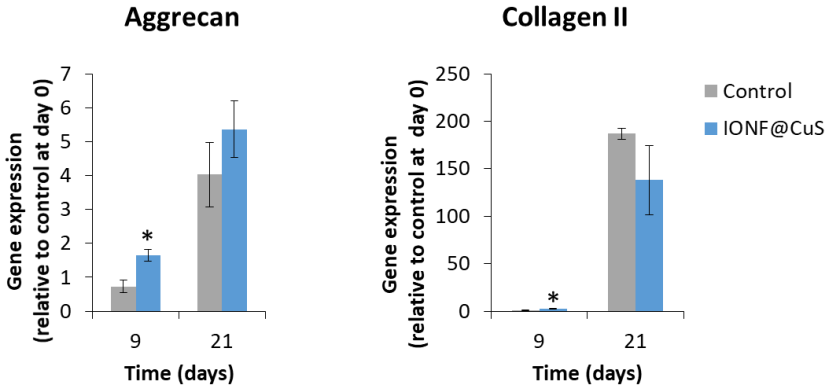

Figure S8: Gene expression of aggrecan and collagen II of spheroids labeled with IONF@CuS at day 9 and 21, relatively to control spheroids at day 0 (*$p<0.05$).

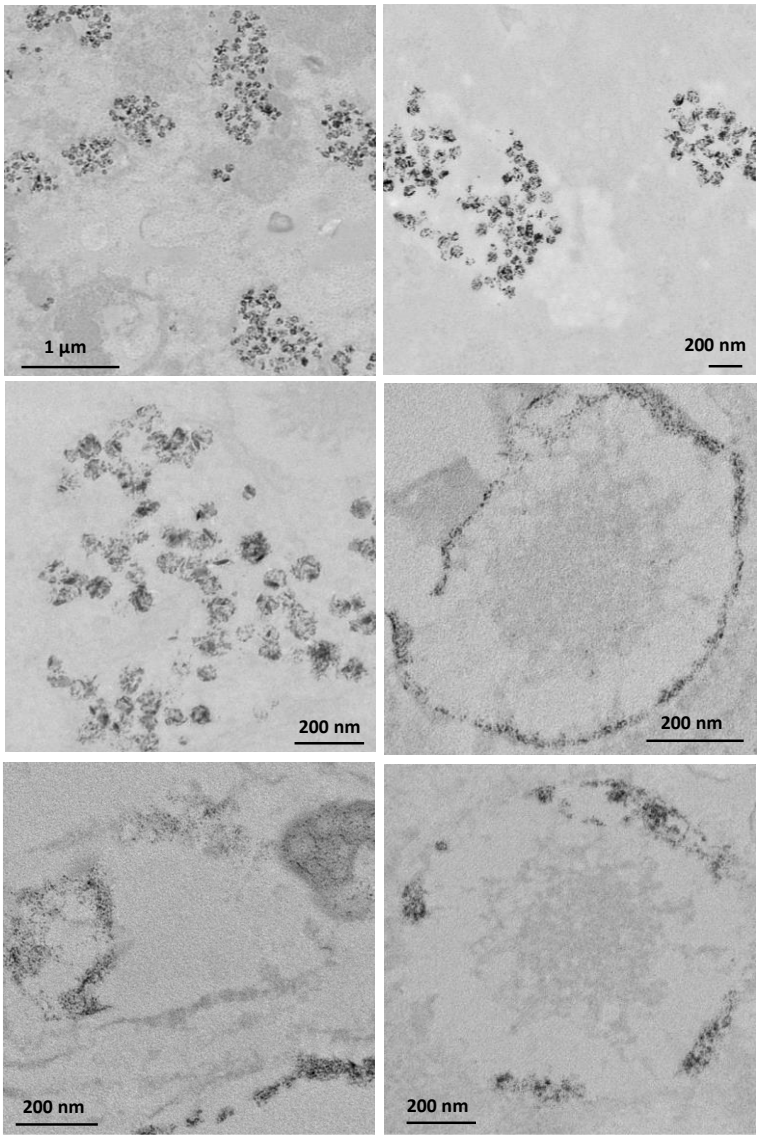

Figure S9: Follow-up of the internalized CuS nanoassemblies after 3 days of spheroid maturation by TEM. It is still possible to spot almost pristine nanoassemblies enclosed in the endosomes, but also some structures resembling more to late endosomes-lysosomes containing more digested nanomaterial. The degradation products are organized in a different way, more accumulated to the organelle walls, huddled against the inner side of the endosomal membrane.

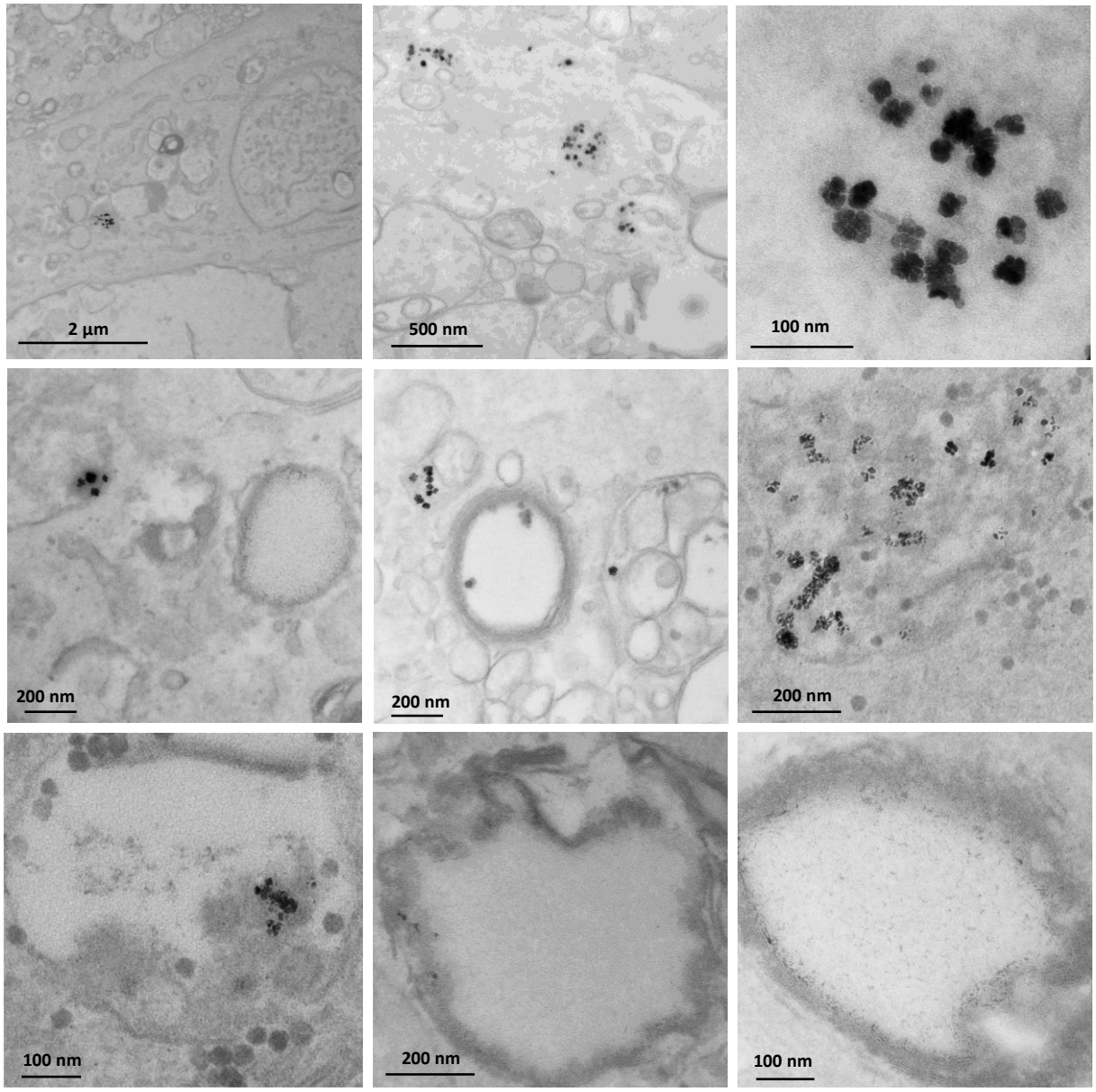

Figure S10: Follow-up of the internalized IONF@CuS nanoassemblies after 3 days of spheroid maturation by TEM. It is possible to find the IONF@CuS nanoassemblies intact inside the endosomes, especially the IONF core, but also there are some organelles where the material is more degraded and absorbed to the inner membrane. It seems also that a compartmentalization is occurring between the Cu and the Fe part processed separately.

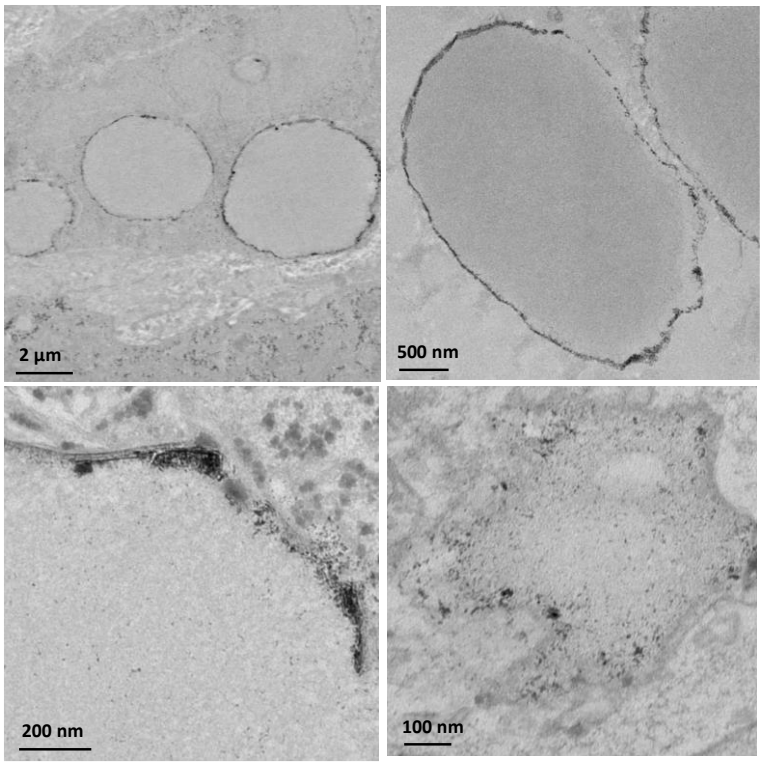

Figure S11: TEM observation of CuS NPs after 21 days of spheroid maturation. The NPs appear extensively re-shaped. There is a prominent accumulation of the material on the walls of the endosomes, as well as organelles filled with newly formed small nanoparticles.

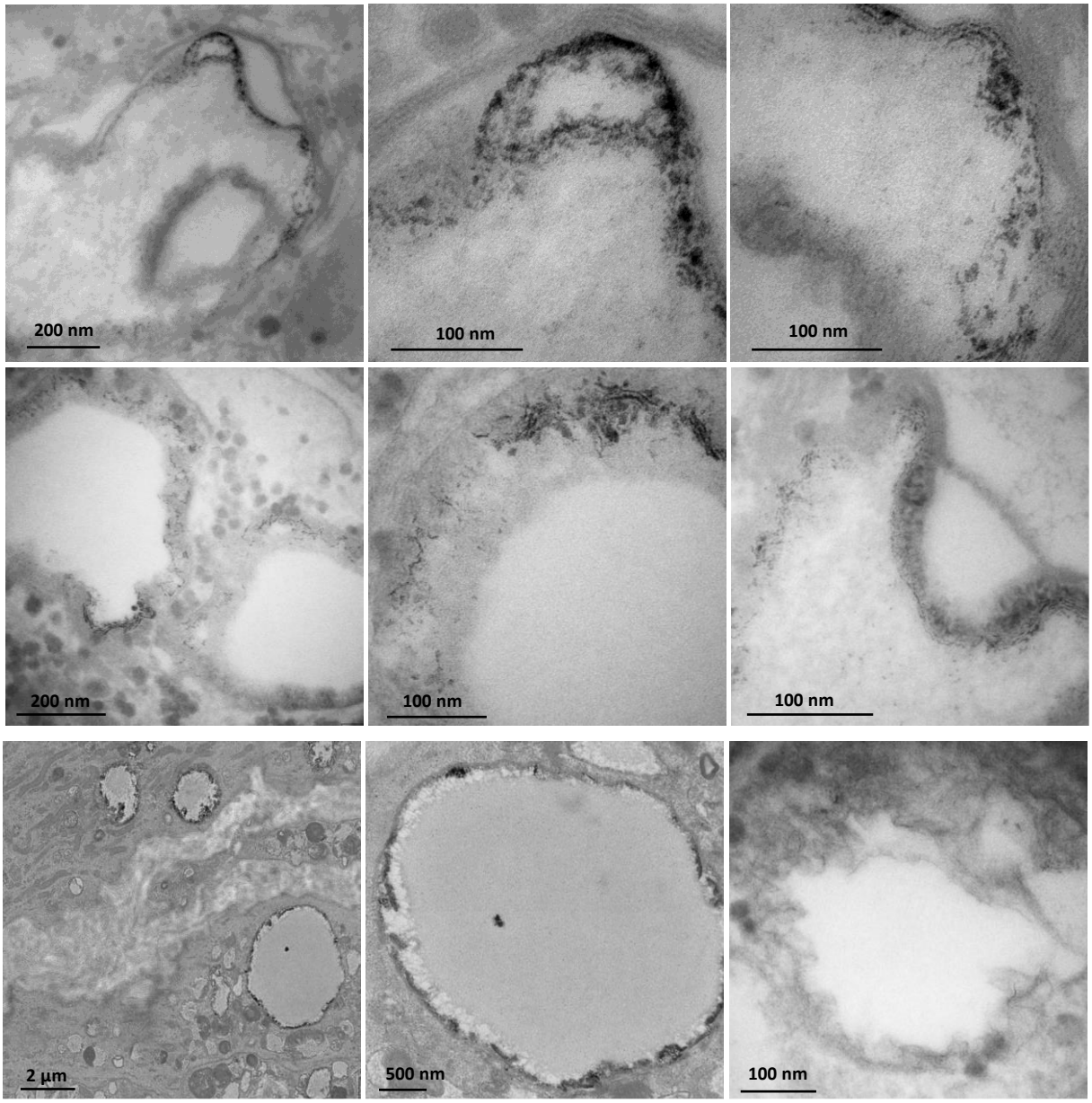

Figure S12: TEM observation for IONF@CuS labeled cells at day 9 (first 2 lines) and at day 21 (last line). The majority of the NPs has been re-shaped, in particular forming membrane associated structures that were visible also for CuS NPs.

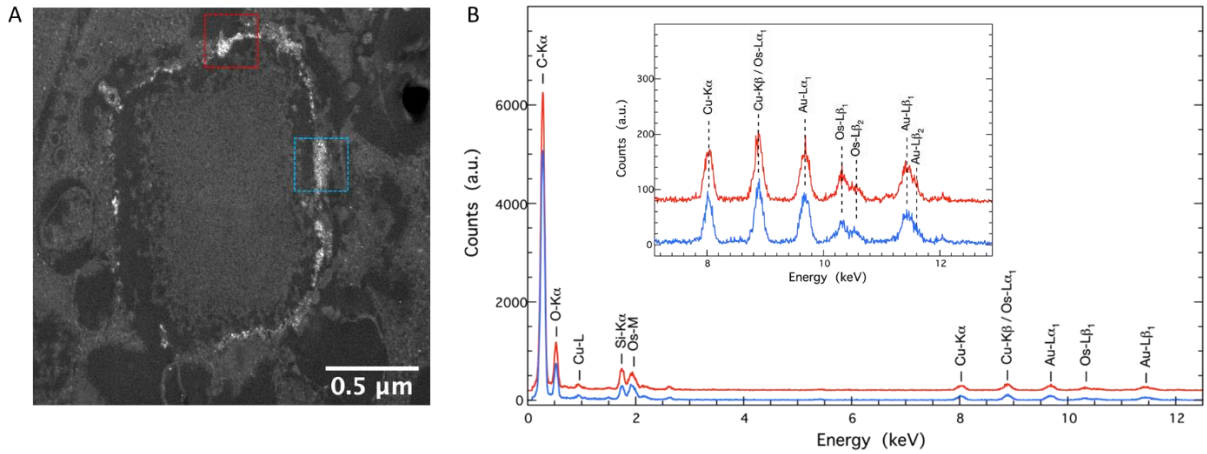

Figure S13: Electron microscopy characterization of the CuS nanoassemblies 21 days after internalization in stem cell-spheroids. A) Scanning TEM in High-angle annular dark-field imaging mode (STEM-HAADF) of a lysosome evidences higher atomic number elements, which can correspond to copper, accumulated along the membrane of the lysosome. B) Energy-dispersive X-ray spectroscopy (XEDS) elemental analysis of the material observed in the two areas identified in image A confirms the presence of copper, issued from the biotransformation of the CuS nanoassemblies, along the lysosomal membrane. Among the detected elements, osmium and gold are also present, corresponding to the contrast agent used for sample preparation and to the grid on which the sample was deposited, respectively.

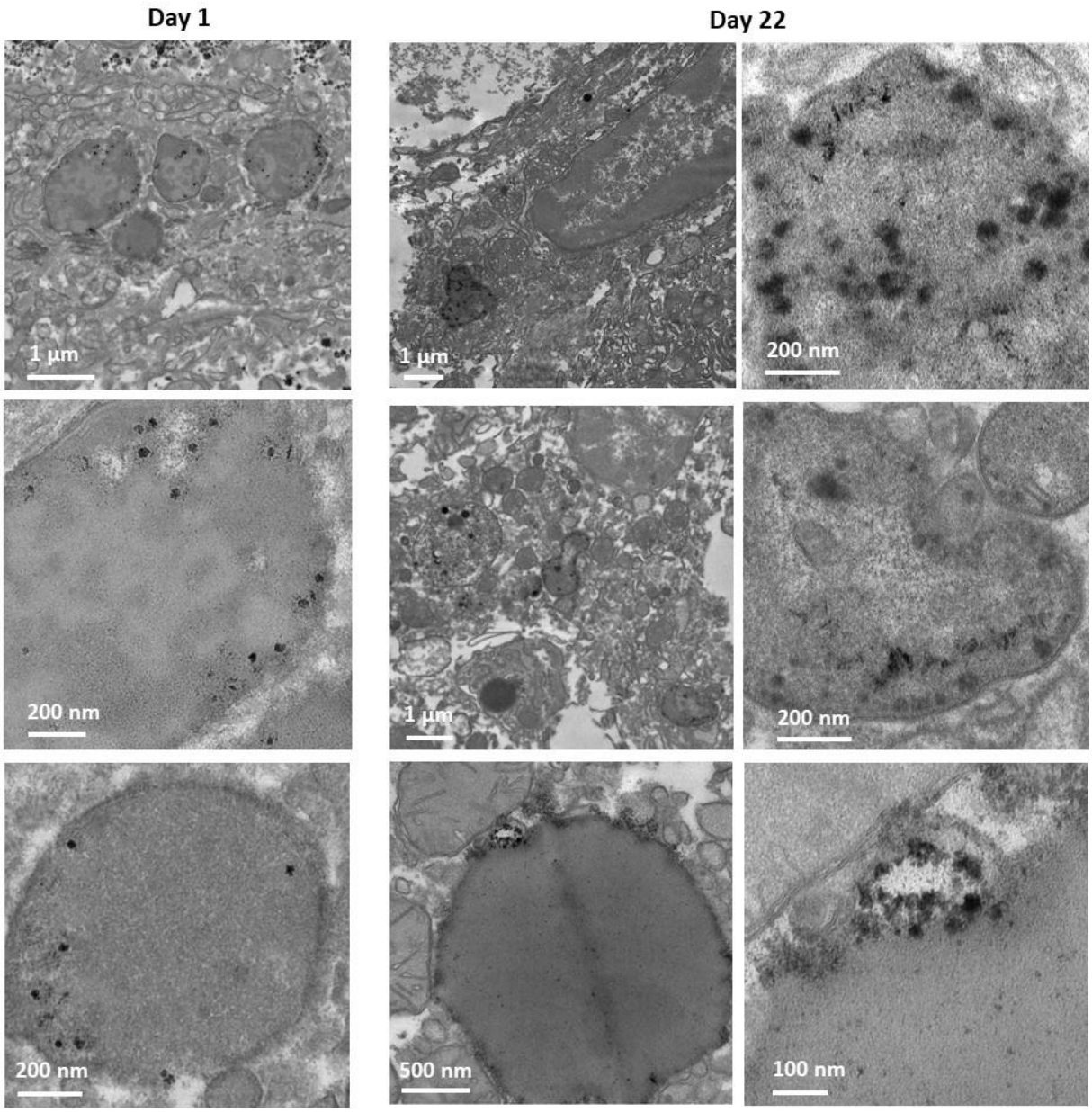

Figure S14: ***In vivo*** **intravenous injection of IONF@CuS NPs and liver TEM observation**. 10 weeks old NMRI-Foxn1-nu/nu mice were injected intravenously with IONF@CuS NPs at a dose of 400 µmol/kg of Cu and 50 µmol/kg of Fe. One day and 22 days after the injection, the mice were euthanized and the livers were collected, rinsed, divided into 1 mm^3 pieces and fixed for 2 h with 4% glutaraldehyde in 0.1 M cacodylate buffer. Then the samples were processed with a microwave tissue processor for electron microscopy. The steps included contrasted with Oolong Tea Extract (OTE) 0.5%, post-fixed with 1% osmium tetroxide and embedded in epoxy resins. Ultrathin slices (70 nm) were collected and counterstained with lead citrate prior to being observed with a Hitachi HT 7700 TEM operated at 80 kV.

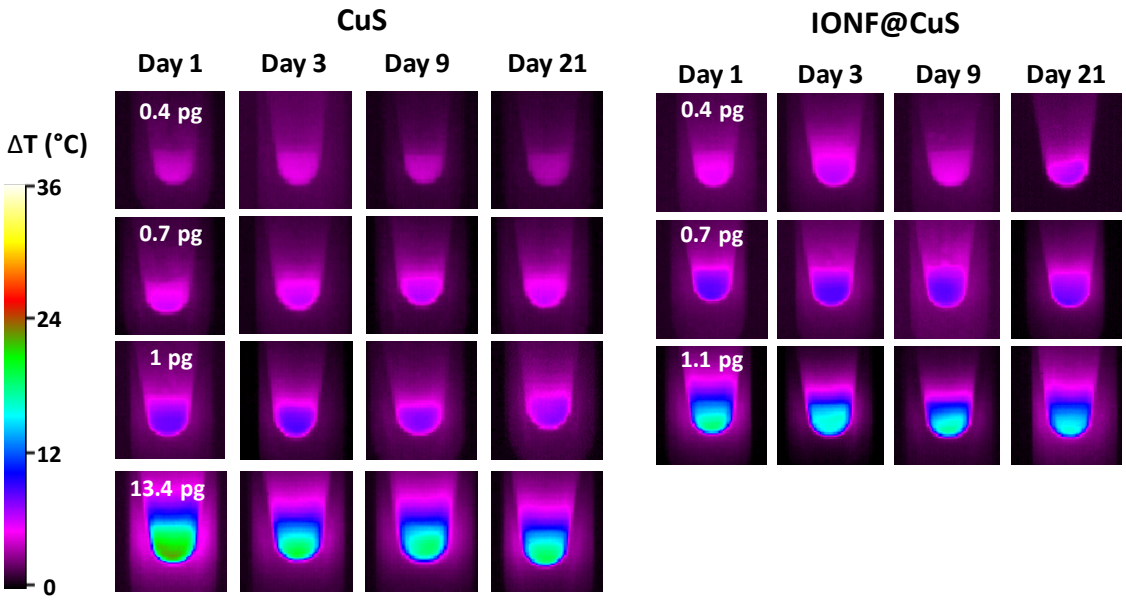

Figure S15: Representative IR images of the spheroids treated with different concentrations of CuS or IONF@CuS nanoparticles resulting in different intracellular amount (pg/cell of Cu reported on each day 1) and irradiated with the 1064 nm laser at 0.3 W/cm^2 after 1, 3, 9 and 21 days of spheroid maturation.

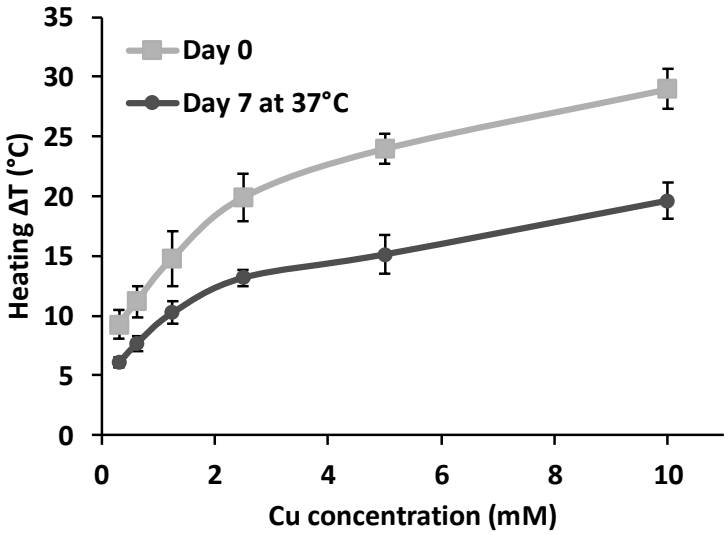

Figure S16: Photothermal analysis of CuS nanoassemblies, as a function of Cu concentration, ranging from 0.3 mM to 10 mM. The NPs suspensions were exposed to the 1064-nm laser (0.3 W/cm^2) either right after dispersion in 100 µL serum-free phenol red-free DMEM culture medium, or later on, after 7 days of incubation at 37°C.

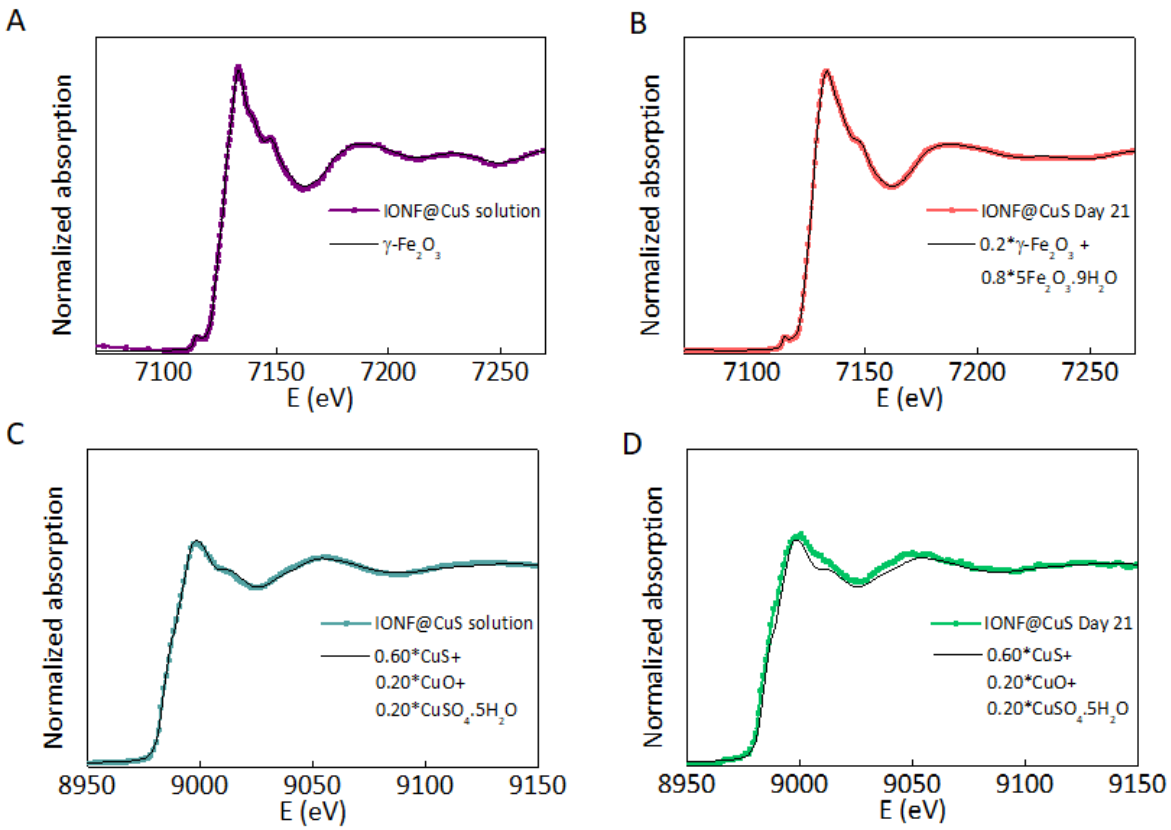

Figure S17: XANES spectra at the Fe K-edge: A) IONF@CuS nanoassemblies in solution and B) IONF@CuS nanoassemblies at day 21. A linear combination fitting has been performed considering iron oxide references. XANES spectra at the Cu K-edge: C) IONF@CuS nanoassemblies in solution and D) IONF@CuS nanoassemblies at day 21. A theoretical linear combination (60 % CuS, 20% CuO and 20% $CuSO_4.5H_2O$) is shown in black for both conditions, adjusting correctly the experimental spectra.

Table S1. List of primers used for the quantification of the gene expression by qPCR.

Gene	Accession Number	Forward Sequence	Reverse Sequence
RPLP0	NM_053275.3	5′ TGC ATC AGT ACC CCA TTC TAT CAT	5′ AAG GTG TAA TCC GTC TCC ACA GA
ACAN	NM_001135.3	5′ TCT ACC GCT GCG AGG TGA T	5′ TGT AAT GGA ACA CGA TGC CTT T
Col2A1	NM_001844.4	5′ ACT GGA TTG ACC CCA ACC AA	5′ TCC ATG TTG CAG AAA ACC TTC A
GLRX	NM_002064.2	5′ TGC AGG AGG GCC CAA GA	5′ AAA TTC CAG AAG CCC TTG TTT G
SOD1	NM_000454.4	5′ CAG GGC ATC ATC AAT TTC GA	5′ TGC TTC CCC ACA CCT TCA C
NOX2α	NM_000101.4	5′ GGG CCC TTT ACC AGG AAT TAC T	5′ GGC ACC GAG AGC AGG AGA T
ATP7A	NM_001282224.1	5′ CAC CAT AAT CAA AAC ATG AGT AAA GAA GA	5′ CTG GCG CTC CAG GAA CAT A
ATP7B	NM_001005918.2	5′ CCT CTC CCG GGA CTT TAA CAC	5′ CCT CTC CCG GGA CTT TAA CAC
SLC7A1	NM_003045.4	5′ GCT CAC ACA CCC TTG TCC AA	5′ AAT GCA TCT ATC ACT GTC CTC TTG AT
ATOX1	NM_004045.3	5′ TGC CGG GTG ATG GTG TTC	5′ GGA AGC TAG GAA GGA ATA GGA CAA
CP	NM_000096.3	5′ GAC ACC ATC AGA GTA ACC TTC CAT AA	5′ CCC CAA TCG GCT CAA TAC TG
DMT1	NM_001174127.2	5′ CAT CGT GGG AGC TGT CAT CA	5′ TTA TTG TTC CGG TTT ACC TGT CTA GA
FerrL	NM_000146.4	5′ CGA ATT GGC CGA GGA GAA	5′ GCC ACG CTG GTT TTG CAT
FerrH	NM_002032.3	5′ TGG CTT GGC GGA ATT TCT GT	5′ TG GCT TGG CGG AAT TTC TGT
MT1E	NM_001363555.2	5′ GGC TCC ATT CTG CTT TCC AA	5′ GCT GGA GCT CAC ACC AGT GA
MT1X	NM_005952.4	5′ TGT CCC GCT GCG TGT TTT	5′ TTC GAG GCA AGG AGA AGC A
MT2A	NM_005953.5	5′ CCC GCT CCC AGA TGT AAA GA	5′ GGT CAC GGT CAG GGT TGT ACA TA
SLC40A1	NM_014585.6	5′ TGG CAT GGG TCT TGC TTT C	5′ GGC GTA CCC TGT GGT GAT G
TfR1	NM_003234.4	5′ GGG ACA GGT GAC CCT TAC ACA	5′ TGA TGA CCG AGA TGG TGG AA
Cyclin D1	NM_053056.2	5′ CGT GGC CTC TAA GAT GAA GGA	5′ CGG TGT AGA TGC ACA GCT TCT C